ELSEVIER

Surface Science 415 (1998) 264–273

surface science

Structure-dependent electrical conduction through indium atomic layers on the Si(111) surface

Sakura Takeda *, Xiao Tong [1], Shozo Ino [2], Shuji Hasegawa

Department of Physics, School of Science, University of Tokyo, Hongo, Bunkyo-ku, Tokyo 113, Japan

Received 12 May 1997; accepted for publication 2 June 1998

Abstract

We have characterized the changes in surface electrical conductance induced by additional indium depositions onto the Si(111)-7×7 clean and the Si(111)-$\sqrt{3}\times\sqrt{3}$-In surfaces at various substrate temperatures by combining in situ electron diffraction and photoemission spectroscopy measurements. On the 7×7 surface, two-dimensional percolation conduction among In microcrystals densely grown on the surface set on around 2.3 ML (monolayer) coverage only below 160 K without any changes in surface structures, while no conductance increase was observed above 160 K up to 40 ML coverage for a lack of percolating paths among sparsely distributed In crystals. On the $\sqrt{3}\times\sqrt{3}$-In surface at room temperature, a drastic increase in conductance was observed accompanying the successive structural changes of $\sqrt{3}\times\sqrt{3}\rightarrow2\times2\rightarrow1\times1\rightarrow\sqrt{7}\times\sqrt{3}\rightarrow1\times1$ structures with an increase of In coverage. This increase was found to be mainly due to the conduction through the In atomic layers grown in a layer-by-layer mode up to 3 ML, though the conduction through the surface space-charge layer also partly contributed to the conductance increase. At lower temperatures, such structural transformations as well as conductance increases were suppressed.

Keywords: Electrical transport measurements; Epitaxy; Indium; Metallic films; Metallic surfaces; Silicon; Surface electrical transport (surface conductivity, surface recombination, etc.); Surface structure, morphology, roughness, and topography; X-ray photoelectron spectroscopy

1. Introduction

Indium atoms of coverages ranging from submonolayer to a few atomic layers deposited on the Si(111) surface are known to exhibit a variety of surface structures [1], and also to be very mobile as revealed in the electromigration phenomena [2]. Such atomistic changes in structures will inevitably raise the changes in electronic transport properties [3–5]. We report here the measurements of surface electrical conductance during In depositions onto the Si(111) surface of its clean 7×7 structure and $\sqrt{3}\times\sqrt{3}$-In structure with various substrate temperatures and deposition rates. Changes in atomic structures and electronic states were also investigated during the deposition by reflection high-energy electron diffraction (RHEED) and X-ray photoemission spectroscopy (XPS). As a result, the electrical conductance was found to be crucially dependent upon the changes in atomic structures and the migration mobility of the deposited In atoms.

* Corresponding author.

[1] Present address: Semiconductor Laboratory, The Institute of Physical and Chemical Research (RIKEN), 2-1 Hirosawa, Wako, Saitama 351-01, Japan.

[2] Present address: Utsunomiya University, 3-5-1 Mine, Utsunomiya, Tochigi 321, Japan.

0039-6028/98/$ – see front matter
PII: S0039-6028(98)00473-7

When In was deposited onto the Si(111)-7×7 surface at low temperatures (around 100 K), the electrical conductance increased due to the percolation conduction among In microcrystals densely formed on the surface, while at room temperature (RT) there was no conductance increase because much larger In islands were formed with much lower number density due to the high mobility of In atoms.

When In was deposited onto the Si(111)-$\sqrt{3}\times\sqrt{3}$-In surface at RT, the conductance dramatically increased corresponding to successive transformations of the surface structures from the $\sqrt{3}\times\sqrt{3}$ to a 2×2, and to a $\sqrt{7}\times\sqrt{3}$ superstructures. From the calculation of the excess carrier concentrations in the surface space-charge layer due to the band bending which was measured by XPS, the observed increases in conductance were found to be too large to be explained only by the band bending. We concluded that the observed conductance increase was mainly due to the conduction through In atomic layers grown in a layer-by-layer mode. As lowering the temperatures down to 100 K, the migration mobility of the In adatoms and resulting structural changes were suppressed, so that the increase in conductance was suppressed. At temperatures lower than 100 K, the conductance through In microcrystals set on without any changes in superstructures in a similar way as on the 7×7 surface around 100 K.

2. Experimental

The experiments were performed in two separate ultrahigh vacuum (UHV) systems with base pressures under 1×10^{-10} Torr. The electrical conductance measurements were done in a chamber containing a RHEED system. The RHEED observations were done during the separate runs of deposition, because the electron beam seriously disturbed the electrical measurements. The sample holder with a liquid-nitrogen container was equipped and the temperature of the substrate was varied from 1500 to 88 K. The conductance was measured by a four-probe method with probes of 0.2 mm $\varnothing$ tantalum wires elastically contacted with the surface of the central part of the Si substrate. In the measurements DC current varying from -100 to 100 μA with five steps at four-second intervals was used. The I–V relations were linear in good accuracy through the measurements, so we employed the coefficients of linear fit for each I–V relation as conductance.

X-ray photoemission spectra were measured in another UHV chamber with a RHEED apparatus. We used a non-monochromated Mg Kα line ($h\nu=$ 1253.6 eV) as the X-ray source. This X-ray had a width of about 0.68 eV in energy because of Mg, Kα_1 and Kα_2 lines with a distance in the energy spectrum of almost 0.3 eV, each having a lifetime broadening of about 0.36 eV [6]. However, the energy resolution of the energy analyzer was about 0.1 eV, so the peak shifts in the spectra could be determined by about ±0.05 eV precision.

The Si substrate was p-type (B doped) of 20 Ω cm resistivity at RT and 35 mm × 4 mm × 0.4 mm in size. The samples used in both chambers were cut from the same Si water. To obtain the clean Si(111)-7×7 surface, the sample was flashed up to 1470 K by the direct-current heating method. Another surface, Si(111)-$\sqrt{3}\times\sqrt{3}$-In, was prepared by depositing In of 1/3 ML (monolayer) onto the 7×7 surface maintained at 800 K, followed by cooling down. The In deposition rate was monitored with a quartz oscillator.

3. Results and discussion

3.1. On the Si(111)-7×7 surface

Fig. 1a shows the conductance change $\Delta\sigma=[(1/R)-(1/R_o)](L/W)$ during In deposition onto the Si(111)-7×7 clean surface at RT and 100 K, where R is the resistance at each In coverage, R_o is the initial resistance, W is the width of the wafer and L is the length of the measured area. At RT, there is no change up to an In coverage of 40 ML, while at 100 K, the conductance steeply rises up around 2.5 ML (see inset in Fig. 1a) and increases monotonically. The RHEED patterns at the two substrate temperatures were also different; at the initial stage of the deposition, the (7×7)

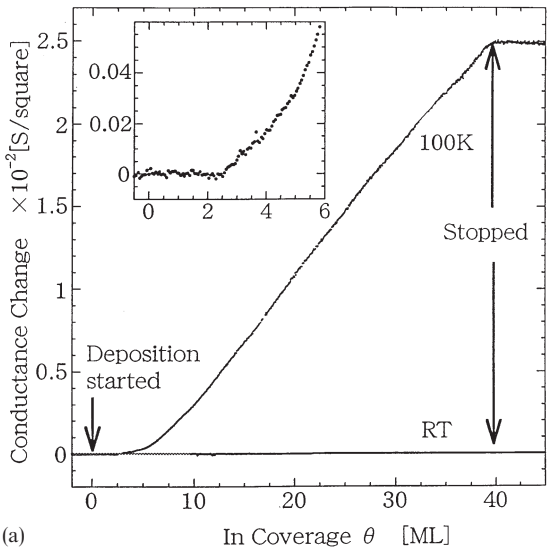

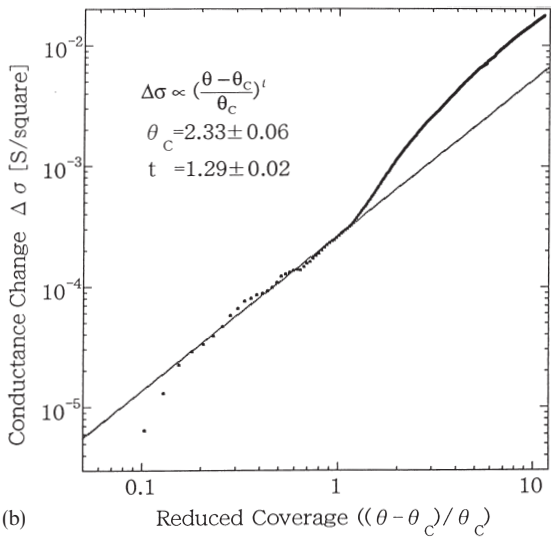

Fig. 1. (a) Conductance change $\Delta\sigma$ measured during In depositions onto the Si(111)-7×7 substrate at RT and 100 K. The inset shows a magnified curve around a critical coverage of 2.33 ML for 100 K measurement. (b) Conductance change $\Delta\sigma$ during In deposition onto the Si(111)-7×7 surface at 100 K as a function of a reduced In coverage. The straight line presents a fitting to the form $\Delta\sigma \propto (\theta-\theta_c/\theta_c)$.

fraction-order spots were weakened gradually and disappeared around 2 or 3 ML for both temperatures, just leaving the Si fundamental 1×1 spots. With further deposition onto the RT substrate, extra streak-like spots appeared just outside the Si bulk fundamental spots. These extra spots indicate the growth of indium islands whose surfaces have a hexagonal structure with lattice constant 3.4 Å and have the same orientation as the substrate. The structure of bulk indium has a face-centered tetragonal structure and its (111) face has a distorted hexagonal structure with lattice constants 3.25 Å and 3.38 Å. So the surface structure of In islands is regarded as a pseudomorphic structure very similar to the (111) surface of bulk In.

Indium on the 7×7 surface at RT is known to grow in the Stranski–Krastanov (S–K) growth mode [7,8]; the first monolayer of In covers the surface, and then three-dimensional (3D) In islands begin to grow. STM observations [7,8] indicate that the large In islands sparsely distribute on the surface at RT and that the surface of these In islands has hexagonal structure with lattice constant 3.29 Å and standard deviation 0.22 Å, which is consistent with our RHEED observation.

At 100 K, on the other hand, broad steaks came out in the RHEED pattern, which were typical patterns from a mosaic structure. This pattern indicated that the islands became much smaller in size and higher in their number density and were spread on the surface as nanometer-sized flat islands. The growth morphology was confirmed by our low-temperature scanning tunneling microscopy, which will be published elsewhere.

It is then expected that the conductance rise from around 2.5 ML at 100 K is due to the In fine islands connecting to each other to form conducting paths on the surface. This path-forming process can be described by the percolation theory [9] which predicts the conductance increase $\Delta\sigma$ as a function of coverage θ in the form

$$\Delta\sigma \propto [(\theta-\theta_c)/\theta_c]^t,$$

where θ_c is a critical coverage and t is a critical exponent. The exponent t for a two-dimensional (2D) system is obtained to be 1.3 by Monte-Carlo simulations [9–11]. We fitted the early stage of the conductance increase to this form using the reduced coverage $(\theta-\theta_c)/\theta_c$ with t and θ_c as fitting parameters. The exponent t thus obtained depended a little on the value of θ_c, so we tried the fitting for several values of θ_c and searched for

the best combination of θ_c and t to give the smallest fitting error. As a result, we obtained the critical coverage $\theta_c = 2.33(\pm 0.06)$ ML and $t = 1.29 \pm 0.02$, as shown in Fig. 1b. The agreement of our t with that obtained by the simulations insists that the observed conductance increase is a set-on as a 2D percolation among In fine islands.

After islands were percolated, conductance monotonically increased until the shutter was closed at 40 ML. This increase can be attributed to the conductance through a continuous In film. The increase of conductance after about 10 ML can be fitted to a linear equation $\Delta\sigma = a \cdot d - b$ where d is the film thickness and a and b are parameters. In a simple consideration, a can be regarded as a conductivity with a being a coefficient of the film thickness in mind. The conductivity of the film estimated in this way from Fig. 1a is 8×10^{-4}[S/(square · ML)]. This is an order of magnitude smaller than the bulk value at 100 K, 8×10^{-3}[S/(square · ML)]. Assuming the Drude model for the conductance mechanism, although it is a very rough estimation, the mean free path of electrons at the thickness d is estimated with Ref. [12] to be 23 Å in the coverage region from 10 to 40 ML. Since this length is constant with the increase of film thickness, this mean free path would be said to be restricted by the scattering at boundaries of microcrystals or at defects in the film whose sizes and densities are constant during the thickness increase.

The no conductance change up to 40 ML of In deposition at RT is explained by the fact that islands grow in a 3D way with a large separation among them, so the critical coverage is too large to make the percolation paths. The first monolayer in the S–K growth scarcely contributes to the conductance either at RT or at 100 K, which is consistent with two reports that state little band bending occurs during In deposition onto the Si(111)-7×7 surface [13] and that the first monolayer is not a continuous monatomic layer but an ensemble of small In agglomerates uniformly spread over the Si surface [7].

3.2. On the Si(111)-$\sqrt{3} \times \sqrt{3}$-In surface

Fig. 2a shows the conductance change during In depositions onto the Si(111)-$\sqrt{3} \times \sqrt{3}$-In surface at RT. When deposition was started, the conductance increased up to 3 ML coverage with characteristic inflections (indicated by A, B and C in the figure). These inflections were almost coincident to points of the surface structural transformations, $\sqrt{3} \times \sqrt{3} \rightarrow 2 \times 2 \rightarrow$Si-$1 \times 1 \rightarrow \sqrt{7} \times \sqrt{3}$, which were observed by RHEED in the separate runs of depositions. "Si-1×1" means there are no superspots other than Si-1×1 fundamental spots in the RHEED pattern. The conductance increase stopped at around 3 ML of coverage (point D) and no change appeared even with further deposition, where the $\sqrt{7} \times \sqrt{3}$ superspots in RHEED gradually fade out to leave the 1×1-Si fundamental spots and 1×1-In spots. These 1×1-In spots gradually appeared at around 2.5 ML and indicate the existence of In 3D flat island on the surface, which is the same as the case on the 7×7 surface at RT. When In deposition was stopped, the $\sqrt{7} \times \sqrt{3}$ superspots gradually appeared again, and simultaneously the conductance started to decrease. The conductance change by stopping the deposition is shown in Fig. 2b. The deposition was stopped at the point indicated as E in the figure. The conductance decreased soon after and then reached a smaller constant value which is almost the same as that at 2 ML coverage during the deposition. When the deposition was restarted, the conductance increased to the higher constant value again. We measured this conductance change with various deposition rates (0.045–1.125 ML min^{-1}), and confirmed that the inflections appeared in the same way and the amount of conductance changes were the same within an experimental accuracy of about 10%.

At the lower substrate temperatures, the surface structural transformations differed from the RT case. The 2×2 spots were weak on the substrate at 200 K, and not observed below 200 K; the fundamental Si 1×1 spots were just seen in the coverage range where the 2×2 pattern had been observed at RT. The $\sqrt{7} \times \sqrt{3}$ pattern also did not appear below 160 K. At 100 K the initial $\sqrt{3} \times \sqrt{3}$ spots just disappeared around 0.8 ML In coverage without any other superspots appearing, and broad streaks slowly appeared around 8 ML on the 1×1 pattern. These streaks were the same

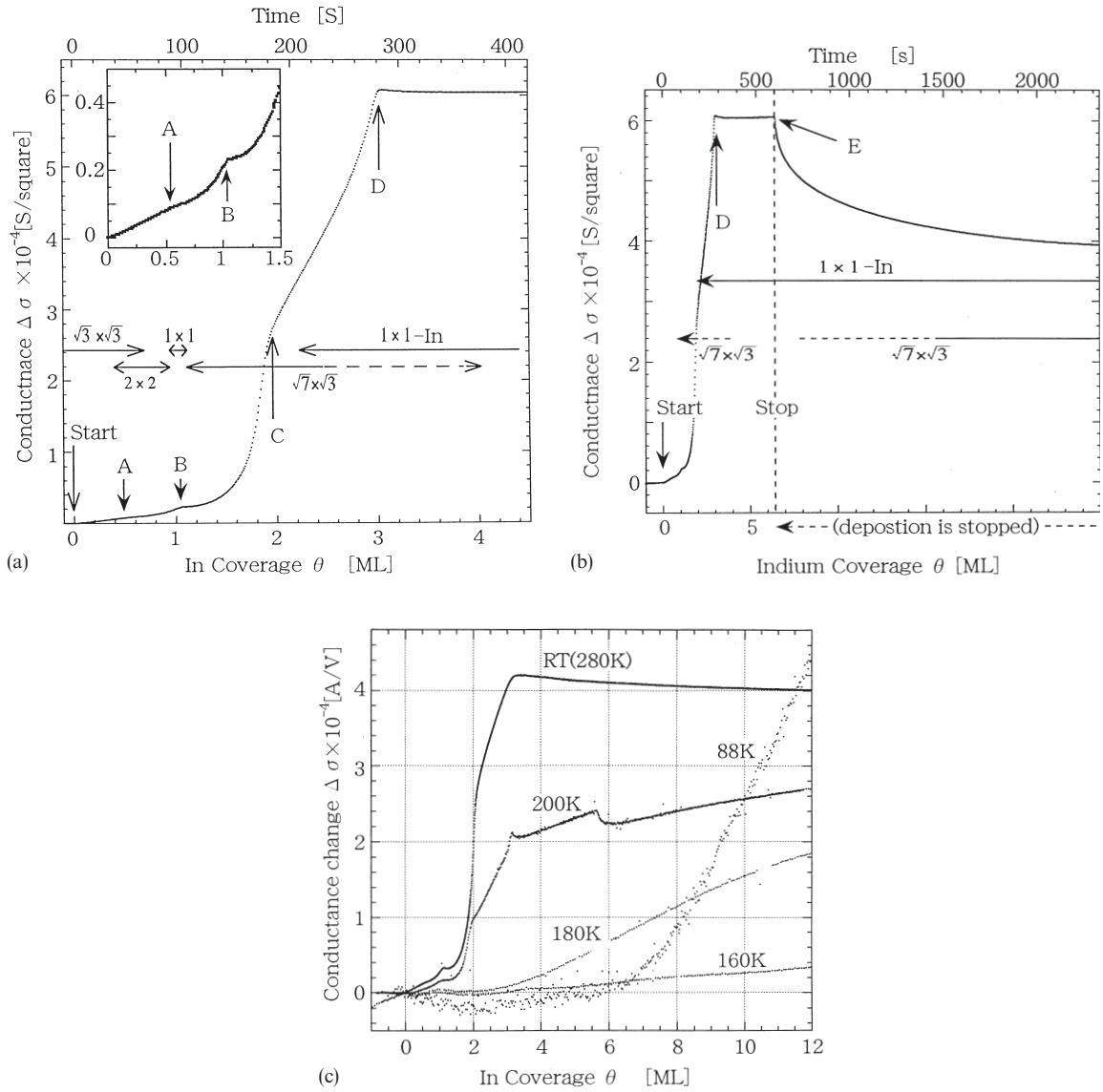

Fig. 2. (a) Conductance change $\Delta\sigma$ and surface structures during In deposition onto the Si(111)-$\sqrt{3}\times\sqrt{3}$-In surface at RT. (b) Conductance change $\Delta\sigma$ and surface structures during and after indium deposition onto the Si(111)-$\sqrt{3}\times\sqrt{3}$-In surface at RT. The structure transformation in the initial coverage range is not shown in this figure since it is the same as that shown in (a). (c) Conductance change $\Delta\sigma$ during In depositions onto the Si(111)-$\sqrt{3}\times\sqrt{3}$-In surface at various substrate temperatures.

as those observed on the 7×7 surface at 100 K, which showed the growth of In microcrystals. The conductance curves for these low temperatures are shown in Fig. 2c. The inflections on the curves at RT and 200 K clearly correspond to the appearance of the 2×2 and the $\sqrt{7}\times\sqrt{3}$ structures. These inflections are not seen below 200 K where no structural transformations were observed. Hence, it is obvious that the characteristic conductance change at RT is associated with the formations and disappearances of the 2×2 and $\sqrt{7}\times\sqrt{3}$ surface superstructures. At 88 K, the conductance

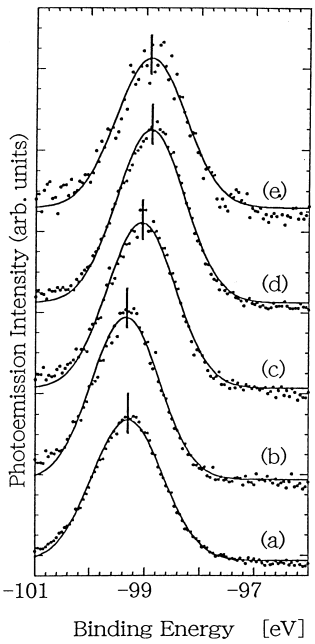

Fig. 3. X-ray photoemission spectra from the Si 2p core level of the (a) 7×7 clean and (b) $\sqrt{3}\times\sqrt{3}$-In surfaces, and (c) 2×2, (d) $\sqrt{7}\times\sqrt{3}$ and (e) 1×1 surfaces which were prepared by depositing In of 0.7, 3 and 5 ML onto the $\sqrt{3}\times\sqrt{3}$ surface at RT, respectively. The peak positions were determined by Gaussian fits.

increase looks similar to the case of the 7×7 substrate in Fig. 1a, indicating the percolation mechanism, though the critical coverage seems different.

In order to furthermore characterize the observed conductance changes at RT, we measured the band bending at the surface space-charge layer in the Si substrate. Fig. 3 shows XPS spectra for the Si 2p core level obtained from (a) 7×7, (b) $\sqrt{3}\times\sqrt{3}$-In, (c) 2×2-In (at additional 0.7 ML In coverage on the $\sqrt{3}\times\sqrt{3}$-In surface), (d) $\sqrt{7}\times\sqrt{3}$-In (at additional 3 ML) and (e) 1×1 (at additional 5 ML) structures at RT, respectively. We must note that the spectrum in (e) for the 1×1 surface structure was measured for a 5 ML In deposited surface. But this surface returned to the $\sqrt{7}\times\sqrt{3}$ structure by stopping the deposition as mentioned in Fig. 2b, where the XPS measurements were carried out. The binding energy is referred to the Fermi level, E_F. Since our X-rays of Mg $K\alpha_{1,2}$ lines were not monochromized, the peaks of $2p^{1/2}$ and $2p^{3/2}$ were not resolved. But the shifts of the convoluted peaks could be detected with about ±0.05 eV accuracy by fitting data analysis. As seen between (b)–(e) in the figure, the energy of the Si 2p level shifts towards E_F with In coverage increasing on the $\sqrt{3}\times\sqrt{3}$-In surface. Emitted photoelectrons in our case have such a high kinetic energy (about 1.2 keV) that their escape depths are about 20 Å estimated using a so-called "universal curve" for the electron's escape depths in materials as a function of its energy [14]. So the photoelectrons are almost free from any surface chemical shifts. This escape depth is, however, shallow enough to examine the E_F position at the surface, because the Si band bending in the surface space-charge layer of our Si crystal extends over 2000 Å [15] which is much longer than the escape depth. Therefore, the observed energy shifts of the Si 2p core level directly correspond to the band bending under the surface. The shifts of the Si 2p core level relative to the $\sqrt{3}\times\sqrt{3}$-In surface are (c) 0.28 ± 0.05 eV, (d) 0.47 ± 0.05 eV and (e) 0.50 ± 0.05 eV.

It is known that the energy distance E_F-E_{VBM}, where E_{VBM} is the valence-band maximum at the surface, is measured to be 0.63 eV for the 7×7 surface [16]. The Si 2p peak of the $\sqrt{3}\times\sqrt{3}$-In surface is located at a position deeper than that of the 7×7 surface by 0.03 ± 0.05 eV (compare Fig. 3a and 3b). Then, it is simply obtained from the XPS results that the E_F-E_{VBM} for the respective surface structures are (b) 0.66 ± 0.5 eV, (c) 0.38 ± 0.5 eV, (d) 0.19 ± 0.05 eV and (e) 0.16 ± 0.05 eV. Since, at the (d) $\sqrt{7}\times\sqrt{3}$ and (e) 1×1 surfaces E_F's are located near E_{VBM}, the surface space-charge layer becomes a hole-accumulation layer. On the other hand, the layers under the (c) 2×2 and the (b) initial $\sqrt{3}\times\sqrt{3}$ surfaces are depletion layers as in the case of the 7×7 surface.

We now discuss the mechanism of the conductance changes in Fig. 2a according to the surface structural transformations. There are three possibilities to account for the conductance change [4], which are a conductance through the surface-state band, that through the grown metal atomic layer and that through the surface space-charge layer of the substrate. The distinction between the former

two types of conductance will be obscure when the metal overlayers around monolayer thicknesses make surface superstructures like the present case of the In layers.

The above XPS results show that the band bendings occur for the respective structures. We then estimate the increase of the carrier concentration induced by the band bendings. The change of carrier concentration Δn_{sc} in the surface space-charge layer referred to that under the flat-band condition was calculated under the respective band bendings using the modified Poisson equation as follows [17]:

$$\Delta n_{sc} = \pm L_D n_i \int_{u_s}^{u_b} [(e^{\pm u} - e^{\pm u_b})/\sqrt{2}[\cosh(u) - \cosh(u_b) + (u_b - u)\sinh(u_b)]^{1/2}]\, du,$$

where L_D is the Debye length, n_i is the intrinsic carrier concentration for silicon, $u_b = (E_F - E_{mb})/K_B T$, $u_s = (E_F - E_{ms})/K_B T$, E_m is the middle of the band gap which changes depending on the distance from the surface under the band bending condition, and suffixes b and s are for their values in deep bulk and at the surface, respectively. We use the band gap energy to be 1.1 eV [18], so $E_F - E_{ms} = -0.55 + (E_F - E_{VBM})$. The plus signs at exponents in the numerator of the integrand stand for conduction electrons and minus signs are for conduction holes. A plus sign put before L_D is for the case of $u_s > u_b$ (downward band bending), while a minus sign before L_D is for $u_s < u_b$ (upward band bending). The carrier concentration change Δn_{sc} thus obtained is converted to the conductance change $\Delta\sigma_{sc}$ through the simple relation $\Delta\sigma_{sc} = e \times (\Delta n_{HOLE} \times \mu_{HOLE} + \Delta n_{ELE} \times \mu_{ELE})$, where μ_{HOLE} and μ_{ELE} are the mobilities of holes and electrons. The curves in Fig. 4 show $\Delta\sigma_{sc}$ calculated as a function of the surface E_F position, obtained using the bulk values for the mobilities of holes and electrons, which are 496 and 1330 $cm^2\,V^{-1}s^{-1}$, respectively [18]. The four curves are calculated by assuming different resistivities of Si crystal, corresponding to a different E_F position in the bulk. This is for later discussions on possible reduction or accumulation of impurities in the bulk (subsurface region) due to heat treatments. Then, we can estimate the conductance increases

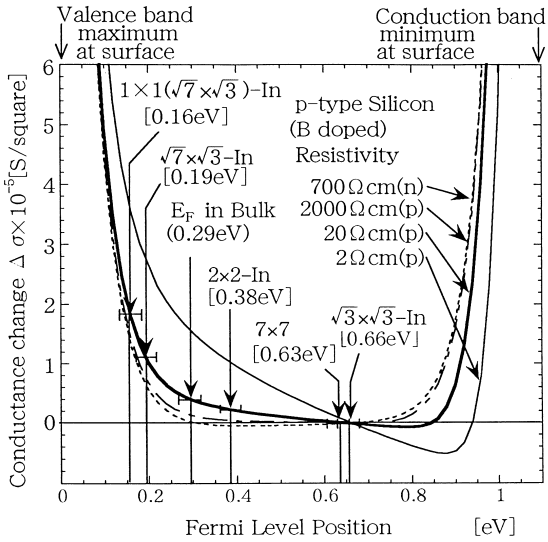

Fig. 4. The excess conductance $\Delta\sigma_{sc}$ through the surface space-charge layer in the substrate, calculated as a function of the surface-Fermi-level position measured from the valance-band maximum. The conductance at the $\sqrt{3}\times\sqrt{3}$-In surface is defined as a reference. The E_F positions at the respective superstructures determined by XPS measurements are indicated. The energy in square brackets has an error of ± 0.5 eV. Thin-solid, thick-solid, dash and dot-dash lines show the calculations for 2 Ω cm (p-type), 20 Ω cm (p-type), 2000 Ω cm (p-type) and 700 Ω cm (n-type) samples, respectively. These resistances correspond to the E_F positions in the bulk at 0.02, 0.29, 0.40 and 0.66 eV above E_{VBM}, respectively.

through the surface space-charge layer at the respective surface structures as a function of the surface E_F positions determined by XPS measurements. The conductance increases for the 2×2 and $\sqrt{7}\times\sqrt{3}$ surfaces with respect to at the $\sqrt{3}\times\sqrt{3}$ surface (designated as $\Delta\sigma_{SC}^{2\times2}$ and $\Delta\sigma_{SC}^{\sqrt{7}\times\sqrt{3}}$ here after) are estimated to be $\Delta\sigma_{SC}^{2\times2} = 2.3(\pm0.3)\times10^{-6}$[S/square] and $\Delta\sigma_{SC}^{\sqrt{7}\times\sqrt{3}} = 1.2(\pm0.4)\times10^{-5}$[S/square] (or $1.9(\pm0.4)\times10^{-6}$ [S/square] if one takes the Fermi level position at the 1×1-In surface in Fig. 4), respectively. On the other hand, the measured conductance increases for the respective surfaces in comparison to the conductance of the initial $\sqrt{3}\times\sqrt{3}$-In surface are $\Delta\sigma_{2\times2} = 2.3(\pm0.1)\times10^{-5}$[S/square] (see Fig. 2a) and $\Delta\sigma_{\sqrt{7}\times\sqrt{3}} = 3.8(\pm0.2)\times10^{-4}$[S/square] (we take the value of $\Delta\sigma_{\sqrt{7}\times\sqrt{3}}$ as a smaller constant value after the deposition off in Fig. 2b, so that we can consistently compare the conductance increase

with the XPS results), respectively. The measured $\Delta\sigma_{2\times2}$ is about 10 times larger than the space-charge layer contribution $\Delta\sigma_{SC}^{2\times2}$, and $\Delta\sigma_{\sqrt{7}\times\sqrt{3}}$ is about 20–30 times larger than $\Delta\sigma_{SC}^{\sqrt{7}\times\sqrt{3}}$. This discrepancy seems to suggest that mechanisms other than the space-charge layer are responsible for this conductance change. If one takes into account that the mobilities of carriers in the surface space-charge layer can be smaller than the bulk values due to carrier scattering at the surface in the case of steep band bending, the discrepancy between the respective $\Delta\sigma$ and $\Delta\sigma_{sc}$ will become more serious. Furthermore, the possibility that some changes in the dopant concentration near the surface region, which may be caused by high-temperature flashings and annealings in vacuum [19,20], must be considered. For such a case, we calculate $\Delta\sigma_{sc}$ changes assuming samples of several resistivities. The results are shown in Fig. 4 by four curves. As seen in the figure, the calculated $\Delta\sigma_{sc}$ changes by a factor of less than three at most even if the resistivity changes from a nominal value (20 Ω cm) by two orders of magnitude. This means the conductance change is not explained by space-charge-layer conduction even if assuming some changes in the dopant concentration near the surface region. From these considerations, it can be said that the band bending in the surface space-charge layer is not a major reason for the observed conductance increase.

As a possible main reason for it, the conductance through In atomic layers or through the surface-state band remains.

The correspondence between characteristic features in the conductance changes that are indicated A and B in Fig. 2a and the structure transformations suggests that the structure transformations affect the surface conductance. The stop of the conductance increase at 3 ML (marked C in Fig. 2a) and the following constant conductance in spite of further deposition seem to indicate the occurrence of 3D island growth from this coverage. The conductance change and the RHEED pattern depended on interruptions and restarts of deposition. It is summarized as follows. The conductance of the high constant value was achieved only during deposition where the RHEED pattern showed almost only the 1×1-Si and the 1×1-In spots. The $\sqrt{7}\times\sqrt{3}$ spots were seen at the initial stage of the region where conductance was at the high constant value, but faded out within 1 ML after the conductance reached the high constant value. And during interruption of deposition, the conductance gradually decreased to the lower constant value corresponding to that around 2 ML coverage during deposition, and $\sqrt{7}\times\sqrt{3}$ spots gradually appeared in the RHEED pattern.

To explain these phenomena, we propose the following mechanism. The deposited In on the $\sqrt{3}\times\sqrt{3}$-In surface grows as Stranski–Krastanov growth mode, the first 3 ML grow as layer-by-layer growth mode and then followed by the island growth mode. The first two atomic layers are pseudomorphic films; the first layer has a 2×2 superstructure and the second layer has a $\sqrt{7}\times\sqrt{3}$ superstructure. The third layer showing the 1×1 structure, which is an intermediate layer between layer-by-layer growth mode and island growth mode, is kinetically meta-stable only during deposition. Once the deposition is interrupted, the third layer aggregates into 3D islands, the remaining underlying first two layers showing the $\sqrt{7}\times\sqrt{3}$ structures. When the deposition is restarted, the third layer is provided again by the arriving In atoms. The meta-stable 1×1 phase is more conductive than the stable $\sqrt{7}\times\sqrt{3}$ phase. So the disappearance and the appearance of the $\sqrt{7}\times\sqrt{3}$ spots correspond to the formation and the disappearance of the meta-stable third layer and the high constant level and the low constant level of the conductance, respectively. The $\sqrt{7}\times\sqrt{3}$ spots in the RHEED pattern did not disappear exactly at the same time as the stopping of the conductance increase at 3 ML coverage, but they disappeared submonolayer after that. This may be due to the effect of the RHEED beam. Indium is known to be significantly influenced by electrical field and current as revealed by electromigration phenomena or structure transformations induced by an electric field produced by an STM tip [21–23]. Taking account of these, it seems likely that the RHEED beam affects formation of the meta-stable third layer, and as a result, the third-layer growth may be delayed on the area

where the RHEED beam is irradiated, leaving the surface as the $\sqrt{7}\times\sqrt{3}$ structure.

A surface showing a $\sqrt{7}\times\sqrt{3}$ periodicity is known to appear not only by indium deposition onto the Si(111)-$\sqrt{3}\times\sqrt{3}$-In substrate at RT as described in this paper, but also onto the Si(111)-7×7 surface at elevated temperatures (670–820 K) [7,8,21,22,24,25]. Hereafter, we call the former structure $\sqrt{7}\times\sqrt{3}$ (RT), and the later structure $\sqrt{7}\times\sqrt{3}$ (HT). Although there is no general consensus until now whether the $\sqrt{7}\times\sqrt{3}$ (RT) and the $\sqrt{7}\times\sqrt{3}$ (HT) are the same structures or not, we describe below the reported character of the $\sqrt{7}\times\sqrt{3}$ (HT) structure briefly for a comparison with the $\sqrt{7}\times\sqrt{3}$ (RT) studied here.

According to reports [21,26–28], when In is deposited onto the Si(111)-7×7 surface at 670–820 K, the initial 7×7 surface structure successively transforms to $\sqrt{3}\times\sqrt{3}$ (at 0.33 ML), $\sqrt{31}\times\sqrt{31}$ (at 0.5 ML), 4×1 (at 0.5–1 ML) and to $\sqrt{7}\times\sqrt{3}$ (at 1–1.2 ML). Kraft et al. report that there are two types of atomic structure for the $\sqrt{7}\times\sqrt{3}$ (HT) phase which are designated $\sqrt{7}\times\sqrt{3}$-hex. and $\sqrt{7}\times\sqrt{3}$-rect. whose coverages are 1.0 and 1.2 ML, respectively [21,24]. They also report using STM and visible-light microscopy that further deposition of In on the $\sqrt{7}\times\sqrt{3}$ (HT) surface at 400°C causes a formation of the large 3D islands sparsely distributed on the surface because of the large mobility of the arrived In atoms on the surface. The formation of In layer on top of the $\sqrt{7}\times\sqrt{3}$ surface occurred only when the surface was exposed by oxygen, followed with the deposition of additional In at RT to reduce the mobility of In atoms. This high mobility of indium atoms on the $\sqrt{7}\times\sqrt{3}$ (HT) without oxygen is quite similar to that on the $\sqrt{7}\times\sqrt{3}$ (RT) in our study which is indicated by the constant conductance of over 3 ML coverage in Fig. 2a.

As for the $\sqrt{7}\times\sqrt{3}$ (RT) structure, only a few studies have been reported [4,29]. Very recently, Saranin et al. [29] have studied this surface by AES and STM. Their result shows that each structural transformation ($\sqrt{3}\times\sqrt{3}\rightarrow2\times2\rightarrow\sqrt{7}\times\sqrt{3}$) occurs at coverages smaller than our result. A possible reason to explain this discrepancy may be the difference in the experimental procedure; their AES and STM measurements were carried out after deposition which might raise some structural changes from that during deposition, while our RHEED observations were during deposition.

The conductance of three atomic layers of In calculated from the conductivity of its bulk value at RT is 7.5×10^{-3}[S/square]. This is about 12 times larger than our measured value $6.0(\pm0.3)\times10^{-4}$[S/square] (see Fig. 2a). From this value, the electron mean free path in bulk In at RT and in our three-layer film is estimated to be about 65 Å and 5 Å, respectively. Although it is a rough estimation, 5 Å is too small as a distance among scatters, so the surface scattering is considered to give a severe effect on the conductance in our three-layer film. The atomic structure itself of the layers which is different from the bulk In would be another reason for the discrepancy. In the previous subsection, we showed that the In films grown on the 7×7 surface also have a lower conductivity compared with the bulk value. This was due to carrier scattering by defects such as grain boundaries. But for the film grown on the $\sqrt{3}\times\sqrt{3}$-In surface, the surface scattering may dominate over the defect scattering.

When In was deposited onto the Si(111)-4×1-In or -$\sqrt{31}\times\sqrt{31}$-In surface, we did not observe any significant changes in structures and electrical conductance at RT. This is because the initial surfaces are so stable that 3D In islands are just formed very sparsely on the surface from the beginning of additional deposition, due to the extremely high migration mobility of the deposited In atoms, resulting in the lack of electrical connection among the island. By lowering the substrate temperature, the small In islands were formed closer to each other due to the suppression of the In-atom migration, so we observed a set-on of the percolation conduction as in the case of the 7×7 and $\sqrt{3}\times\sqrt{3}$-In substrates at 100 K.

Acknowledgements

This work has been supported in part by Grants-In-Aid from the Ministry of Education, Science, Culture and Sports of Japan, especially through

Grants-In-Aid for Creative Basic Research (Nos. 08NP1201 and 09NP1201) and International Scientific Research Program (No. 07044133) conducted by Professor Katsumichi Yagi of the Tokyo Institute of Technology. We have also been supported by CREST (Core Research for Evolutional Science and Technology) of the Japan Science and Technology Corporation (JST) conducted by Professor Masakazu Aono of Osaka University and RIKEN.

References

[1] V.G. Lifshits, A.A. Saranin, A.V. Zotov, Surface Phases on Silicon, John Wiley and Sons, New York, 1994, p. 247.
[2] H. Yasunaga, A. Natori, Surf. Sci. Rep. 15 (1992) 205.
[3] W. Mönch, Surf. Sci. 63 (1977) 79.
[4] S. Hasegawa, S. Ino, Int. J. Mod. Phys. B 7 (1993) 3817.
[5] V.A. Gasparov, V.V. Bondarev, K.R. Nikolaev, Phys. Low-Dim. Struct. 6 (1995) 45.
[6] M.O. Krause, J.H. Oliver, J. Phys. Chem. Data 8 (1979) 329.
[7] S.L. Surnev, J. Kraft, F.P. Netzer, J. Vac. Sci. Technol. A 13 (1995) 1389.
[8] H. Öfner, S.L. Surnev, Y. Shapira, F.P. Netzer, Phys. Rev. B 48 (1993) 10940.
[9] M. Sahimi, J. Phys. A, Math. Gen. 17 (1984) L601.
[10] K.G. Watson, J. Kougut, Phys. Rep. 12 (1974) 75.
[11] J.M. Younmans, R.B. Stinchcombe, J. Phys. C: Solid State Phys. 11 (1978) 4098.
[12] C. Kittel, Introduction to Solid State Physics, 7th ed., John Wiley and Sons, New York, 1996.
[13] G. Margaritondo, J.E. Rowe, S.B. Christman, Phys. Rev. B 14 (1976) 5396.
[14] W. Mönch, Semiconductor Surfaces and Interfaces, Springer-Verlag, Berlin, 1993, p. 9.
[15] S.M. Sze, Physics of Semiconductor Devices, John Wiley and Sons, New York, 1981, p. 248.
[16] F.J. Himpsel, G. Hollinger, R.A. Pollack, Phys. Rev. B 28 (1983) 7014.
[17] C.E. Young, J. Appl. Phys. 32 (1961) 329.
[18] K. Syouno, Semiconductor Technology I, Tokyo University Publishing, Tokyo, 1976, p. 20 (in Japanese).
[19] L. He, H. Yasunaga, Jpn. J. Appl. Phys. 24 (1985) 928.
[20] M. Liehr, M. Renier, R.A Wachnik, G.S. Scilla, J. Appl. Phys. 61 (1987) 4619.
[21] J. Kraft, M.G. Ramsey, F.P. Netzer, Phys. Rev. B 55 (1997) 5384.
[22] J. Kraft, M.G. Ramsey, F.P. Netzer, Surf. Sci. 55 (1997) L271.
[23] A.A. Saranin, T. Numata, O. Kubo, H. Tani, M. Katayama, K. Oura, Jpn. J. Appl. Phys. 36 (1997) 3814.
[24] J. Kraft, S.L. Surnev, F.P. Netzer, Surf. Sci. 340 (1995) 36.
[25] M.S. Finney, C. Norris, P.B. Howes, E. Vlieg, Surf. Sci. 277 (1992) 330.
[26] M. Kawaji, S. Baba, A. Kinbara, Appl. Phys. Lett. 34 (1979) 748.
[27] M.K. Kelly, G. Margaritondo, J. Anderson, D.J. Frankel, G.J. Lapeyre, J. Vac. Sci. Technol. A 4 (1986) 1396.
[28] S. Park, J. Nogami, C.F. Quate, J. Microsc. 152 (1988) 727.
[29] A.A. Saranin, A.V. Zotov, T. Numata, O. Kubo, K.V. Ignatovich, V.G. Lifshits, M. Katayama, K. Oura, Surf. Sci. 388 (1997) 299.